Contents lists available at ScienceDirect

Science of the Total Environment

Short Communication

Identification of micro- and nanoplastic particles in postnatal sprague-dawley rat offspring after maternal inhalation exposure throughout gestation

Gina M. Moreno [a], Tanisha Brunson-Malone [b], Samantha Adams [a], Calla Nguyen [c], Talia N. Seymore [a], Chelsea M. Cary [a], Marianne Polunas [c], Michael J. Goedken [c], Phoebe A. Stapleton [a,b,*]

[a] Department of Pharmacology and Toxicology, Ernest Mario School of Pharmacy, Rutgers University, Piscataway, NJ 08854, USA
[b] Environmental and Occupational Health Sciences Institute (EOHSI), Piscataway, NJ 08854, USA
[c] Research Pathology Services, Rutgers University, Piscataway, NJ 08854, USA

HIGHLIGHTS

- Plastic particles bioaccumulate in offspring following maternal inhalation of particles throughout pregnancy.
- Nylon particles were visualized in 2-week old male and female offspring tissues using hyperspectral dark-field microscopy.
- These findings highlight the persistence of micro- and nanoplastic particles within maternal-fetal biological systems.

GRAPHICAL ABSTRACT
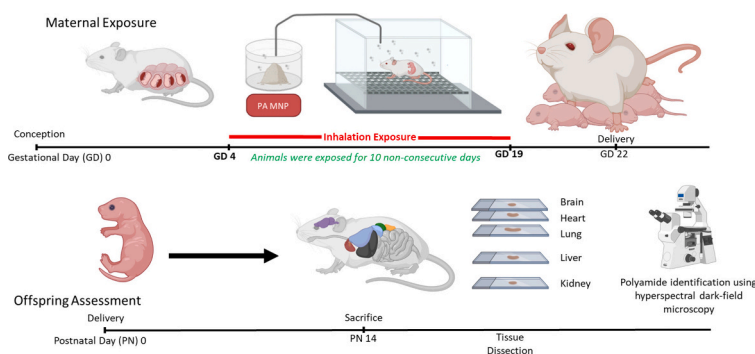
ARTICLE INFO

ABSTRACT

Micro-nanoplastic particulates (MNPs) have been identified in both indoor and outdoor environments. From these real-world exposures, MNPs have been identified in human fluids and organ tissues, including the placenta and breastmilk. Laboratory studies have identified MNPs are capable of crossing the placental barrier and depositing in fetal tissues; however, it remained unclear if MNPs persist in offspring tissues after birth. Six pregnant Sprague-Dawley rats were divided equally into two groups: control and exposed to polyamide-12 (PA-12) MNP aerosols (11.46 ± 3.78 mg/m^3) over an average of 4.35 h ± 0.39 for 10 non-consecutive days between gestational day (GD) 6 – GD 19, in our custom rodent exposure chamber, allowing for whole-body inhalation. Two-weeks after delivery in-house, offspring tissues (i.e. lung, liver, kidney, heart, brain) from 1 male and 1 female pup per litter were fixed in 4 % paraformaldehyde, sectioned, stained with hematoxylin and eosin, and assessed using hyperspectral dark-field microscopy. PA-12 MNPs were identified in all offspring tissues of the exposed dams. No MNPs were visualized in control tissues. These findings have important implications for

* Corresponding author at: Department of Pharmacology and Toxicology, Ernest Mario School of Pharmacy, Environmental and Occupational Health Sciences Institute, Rutgers University, 170 Frelinghuysen Road, Piscataway, NJ 08854, USA.
E-mail address: stapleton@eohsi.rutgers.edu (P.A. Stapleton).

human MNPs translocation, deposition, maternal/fetal health, and the developmental origins of health and disease. Further research is warranted to quantify MNPs mass deposition, biological accumulation, and systemic toxicity.

1. Introduction

Micro-nanoplastic particulates (MNPs) are a ubiquitous environmental contaminant. Microplastics have been defined as plastics <5 mm in dimension, whereas nanoplastic particles are defined as <1000 nm, or 1 μm, in environmental studies and <100 nm in laboratory studies (Stapleton, 2019). These smaller particles are often indirectly produced from the mechanical, thermal, and ultraviolet weathering of bulk plastic materials (Junaid et al., 2024). MNPs are considered a component of particulate matter, and have been identified within air samples acquired from highly populated urban and unpopulated remote locations as well as in food and beverages (Baldwin et al., 2016; Free et al., 2014; Jin et al., 2021; Kosuth et al., 2018; Lenaker et al., 2019; Liao et al., 2021; Mitrano et al., 2021; Toussaint et al., 2019).

MNPs visualization and quantification within human lung samples (Amato-Lourenco et al., 2021; Baeza-Martinez et al., 2022; Jenner et al., 2022) as well as feces (Schwabl et al., 2019) demonstrate unintentional exposure. Recent evidence has identified the translocation of MNPs from these initial pulmonary and gastric epithelial barriers to other physiological systems. MNPs or monomer derivatives of MNPs have been identified within human blood, heart, liver, kidney, and arteries (Horvatits et al., 2022; Leslie et al., 2022; Marfella et al., 2024; Massardo et al., 2024; Yang et al., 2023). Detection of MNPs within these tissues highlights the propensity for MNPs to cross nearly impermeable biological barriers.

MNPs have also been identified in human tissues associated with maternal-fetal health, specifically within placental tissue, fetal meconium, and breastmilk (Braun et al., 2021; Garcia et al., 2024; Liu et al., 2023a; Liu et al., 2023b; Ragusa et al., 2022; Ragusa et al., 2021; Zhang et al., 2021). Interestingly, both humans and rodents are considered hemochorial placental species, wherein the maternal and fetal blood are separated by a cellular layer of cyto- and syncytiotrophoblasts, preventing direct contact between the maternal and fetal circulation (Shojaei et al., 2021). More specifically, humans are hemomonochorial, with a single syncyntiotrophoblast layer; whereas rodents are hemotrichorial, with three cellular layers acting as a barrier between maternal and fetal blood. Previously, we have reported MNPs translocation within a maternal-fetal rodent model (Cary et al., 2023a; Fournier et al., 2020). These studies not only demonstrate particle distribution to the placenta within 24 h after a single maternal pulmonary (Fournier et al., 2020) or gastric exposure (Cary et al., 2023a), but also MNPs deposition within the fetal tissues (e.g., heart, lung, kidney, liver, and brain). However, it was unclear if MNPs remain in offspring tissues after birth.

Therefore, the purpose of the current study was to assess the systemic tissues of neonatal male and female offspring for the deposition of MNPs, after maternal inhalation exposure throughout gestation. Deposition and bio-persistence of MNPs within offspring tissues, after indirect exposure via maternal inhalation, is of great concern as this developmental window may dictate future disease susceptibility.

2. Methods

2.1. Polyamide powder and bulk characterization

Orgasol® 2001 UD NAT 2, a food-grade polyamide-12 (PA-12) ultrafine powder, was obtained from Arkema (King of Prussia, Pennsylvania). Commercial characterization by Coulter Counter identifies PA-12 particles with a spheroid shape and a diameter of 5 ± 1 μm (Arkema, 2004). Physicochemical properties of these particles were previously confirmed in-house via Brunauer-Emmett-Teller specific surface area analysis using the multi-point BET nitrogen adsorption method in the NOVATouch® LX4 surface area and pore size analyzer (Quantachrome Instruments, Boynton Beach, FL) (Cary et al., 2023b). PA-12, more commonly identified as nylon, was selected as a representative MNPs due to identification within human tissues (Amato-Lourenco et al., 2021; Garcia et al., 2024; Ragusa et al., 2022; Yang et al., 2023) and uncommon use within the laboratory and animal care settings.

2.2. Animal model

Six pregnant Sprague Dawley rats were purchased from Charles River Laboratories (Kingston, NY) at Gestational Day (GD) 5. Rats were delivered to an AAALAC accredited vivarium at Rutgers University where they were provided 24 h to acclimate. In the vivarium, food and water were available to the rats ad libitum. Accommodations for the singly-housed dams included a polycarbonate box with wood pellets bedding, filtered water and air, ad libitum food (Purina 508 rat chow), a polycarbonate tube for enrichment, and shredded paper nesting material prior to delivery. Females were randomly assigned to exposure group (naïve or exposure; $n = 3$/group). Maternal MNP inhalations were initiated on GD 6 and ceased after the exposure on GD 19 to allow for nesting and undisturbed partition. Animals delivered in-house and remained in the vivarium with access to food and water ad libitum. All experiments were performed with Rutgers IACUC approval (PROTO999900317; 11/10/2022).

2.3. Inhalation exposure and particle characterization of polyamide aerosol

Bulk food-grade PA-12 powders (Orgasol® 2001 UD NAT 2) were aerosolized using a custom rodent inhalation facility designed for whole-body aerosolized particle inhalation (IEStechno, Morgantown, WV). In brief, particles were aerosolized by an acoustic generator and deliver to an 84 L whole-body exposure chamber as previously described (Baron et al., 2008; Cary et al., 2023b; Fournier et al., 2019). The animal inhalation exposure chamber was connected to state-of-the-art real-time instrumentation in order to detail physicochemical, morphological, and toxicological characterization of the generated and sampled PA-12 aerosol. An time weighted average concentration of near 10 mg/m³ was chosen based on OSHA and American Conference of Governmental Industrial Hygienists limit guidelines for poorly soluble and non-cytotoxic inhalable aerosols, as described in the Safety Data Sheet provided by the manufacturer (Arkema, 2021). Pregnant rats were exposed to aerosolized PA-12 particles (11.46 ± 3.78 mg/m³) over an average of 4.35 h ± 0.39 for 10 non-consecutive days between GD 6 - GD 19, which is comparable to the current average daily concentration assessments of plastic particles in occupational settings (Antti-Poika et al., 1986; Eschenbacher et al., 1999). Final animal exposures took place on GD 19 to reduce animal stress and allow the animal to prepare for delivery. All exposed rats inhaled MNPs aerosols on GD 19, 24 h prior to delivery. Naïve rats ($n = 3$) with no exposure to PA-12 served as controls.

PA-12 aerosol particle size was monitored in real-time using a Scanning Mobility Particle Sizer for aerosols in the nano-range 1–1000 nm (SMPS; TSI Model 3938, Shoreview, MN; set to 12–736 nm), and in a size-fractionated manner using a high resolution electrical low pressure impactor (HR-ELPI+; Dekati, Kangasala, Finland) for submicron- and micron-sized aerosols (0.5–20 μm). The instruments were connected individually on the exposure chamber via flexible and conductive silicone rubber tubing to minimize particle losses. Measurements were

acquired to assess daily inter- and intra-sample variability approximately 1 h after the aerosol generation was started to ensure sufficient time for the particle concentration plateau within the inhalation chamber. Real-time measurements were collected for at least 1 h. The average aerosol size statistics (i.e. median, mode, mean, geometric mean, and geometric standard deviation) were reported (Fig. 1).

Using the MNP size fractionation quantified in this study (Fig. 1), with peaks in the ultrafine (85 nm), fine (0.190 μm) and course (3.07 μm) size ranges, we calculated the predicted deposited particle doses using the Multiple-Path Pulmonary Dosimetry modeling. Deposition and deposition with clearance were modeled with clearance settings based on 4 h/day for 5 day/week for 2 weeks with a one-day post-exposure clearance period. Overall, 99.79 % of the course particles deposited with the respiratory tract, 38.0 % of the fine particulate, and 24.62 % of the ultrafine fraction. Combined, the predicted <u>daily</u>-deposited particle

doses in these regions over the 4 h exposure period were 70.65, 6.14, and 1.45 μg/cm^2, respectively.

2.4. Tissue collection

After humane euthanasia and necropsy on postnatal day 14, the liver, kidney, lung, heart, and brain samples were collected from a representative male and female pup randomly selected from each litter. Lungs were inflated with 4 % PFA using a 26G needle and polycarbonate syringe and tied with braided silk suture. Samples from control and exposed animals were treated in an identical manner, fixed in 4 % paraformaldehyde (PFA) and placed in a polystyrene container.
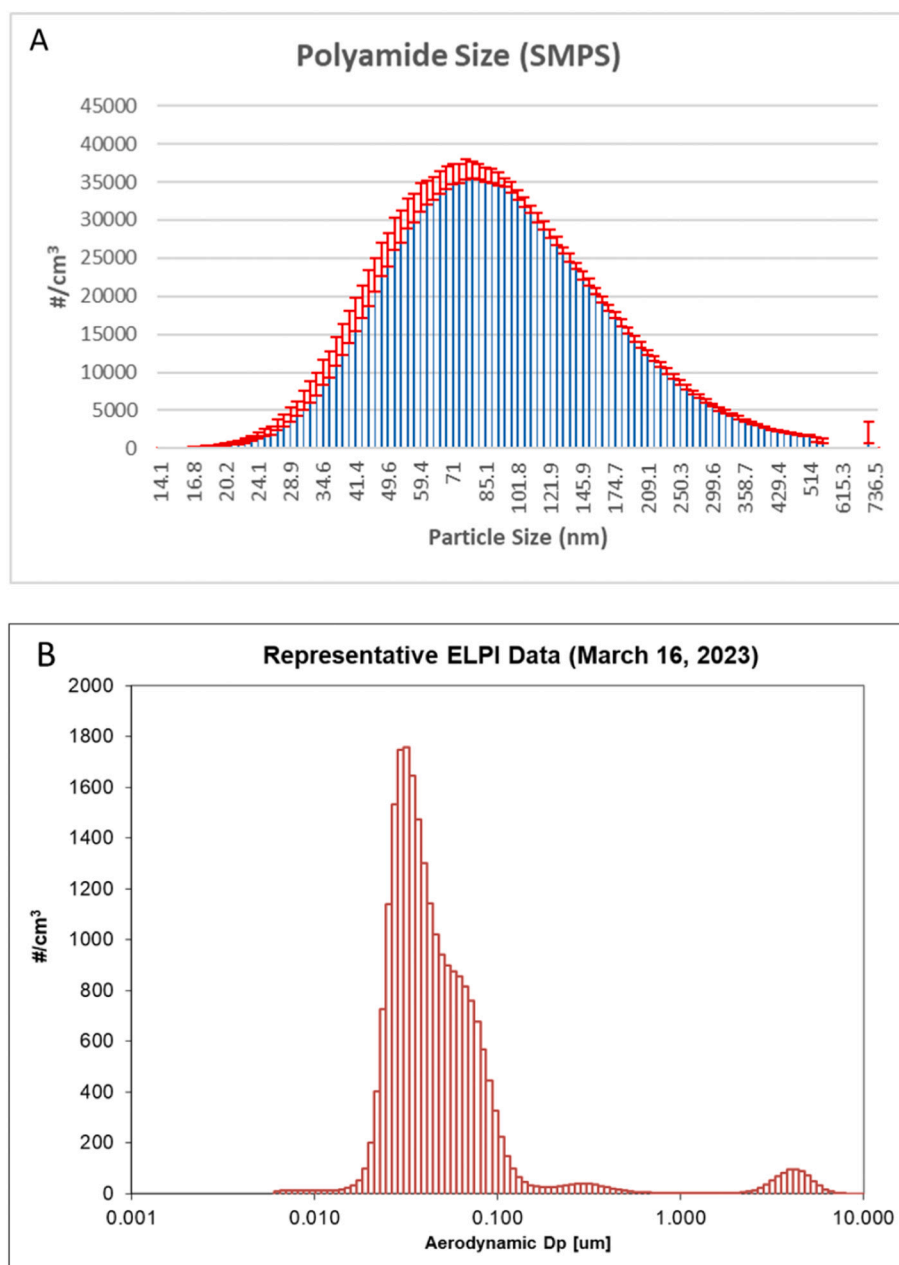

Fig. 1. Real-time size characterization of aerosolized polyamide powder identifies the presence of micro- and nano-scale particles as characterized by electrical mobility (A; SMPS) and aerodynamic diameter (B; ELPI). SMPS data (A) are presented as geometric mean ± SEM for the animal exposures. HR-ELPI data (B) is presented as representative data acquired on March 16, 2023.

2.5. Hyperspectral-enhanced darkfield microscopy

Fixed tissues were transferred to Research Pathology Services. Samples were trimmed, processed, embedded in paraffin. Three slices were taken from the center of each organ: 2 slices were sectioned at 5 μm and one at 15 μm. One 5 μm slice and the 15 μm were unstained for future analyses. The remaining 5 μm slice was stained with hematoxylin and eosin (H&E) for contrast and were visualized via transmitted dark field hyperspectral imaging as previously described (Cary et al., 2023a; Fournier et al., 2020). Scattered light was collected using a 60× oil iris objective (Olympus, Inc). This sample was also evaluated by a board-certified veterinary pathologist for morphometric and histopathological changes associated with gestational exposure.

In brief, CytoViva Enhanced Darkfield Hyperspectral Microscope (EDHM; CytoViva, Inc., Auburn, AL, USA) was used to identify and visualize PA-12, based on the material scattering or emission properties. The system utilizes a tungsten halogen light (Dolan Jenner, Boxborough, MA, USA), with a variable power (0–150 W) control, directed to the microscope via a liquid light guide (Newport Inc., Newport, CA, USA). This light guide connected to the enhanced darkfield illuminator system, mounted onto the condenser of the highly-powered optical microscope, allowed for the angular modification of the light focus onto the focal plane. This indirect oblique illumination allows collection of the reflected or scattered light from the sample, permitting the visual differentiation of objects/materials.

In the EDHM system, the scattered light image from the objective is projected onto a visible and near-infrared (VNIR) diffraction grating spectrograph (Specim, Oulu, Finland), separating the distinct wavelengths of light from 400 to 1000 nm with a spectral resolution of 2 nm. ENVI 4.8 hyperspectral image capture analysis software (Harris Geospatial Solutions, Inc., Herndon, VA, USA) captures and collates the data retrieved by the EDHM charge-coupled device (CCD) video camera (PCO, Kelheim, Germany), in a 10 nm step pixel row by pixel row line scan, to form a hyperspectral image.

The identified PA-12 particles pixels' spectra were captured from to create a spectral library file (SLF). The SLF was then matched to thousands of individual pixel spectra captured from tissues from pups of the exposed dams, for positive matches in the exposed tissues images. A spectral mapping algorithm known as "Spectral Angle Mapper" (SAM) was then utilized to match pixels to the reference spectrum to spectrally map the PA-12 in tissue. Image analysis was conducted to spectrally map PA-12 particles in the tissues. The SLF was then compared to all pixels in the negative control tissue (from pups of control dams) image in a process known as "Filter Spectral Library" to confirm no positive matches.

2.6. Statistics

Student's *t*-test was used to compare animal or litter characteristics. Comparisons of offspring data were made by litter ($n = 3$), not individual pups. Data are presented as mean $\pm$ SEM and significance is set at $p \leq 0.05$.

3. Results

There were no significant differences in the litter characteristics (Table 1) due to the low sample number. Average maternal body weight is 15 % greater in the exposed dams as compared to control ($p = 0.11$), while offspring weight of the exposed group is 20 % smaller than the

controls ($p = 0.16$) with no difference in litter size as defined by pup number ($p = 0.54$). While not significant at this time, these data are consistent with the observed fetal growth restriction that has been previously reported after gestational exposure to aerosolized particulate matter (Cary et al., 2023a; Fournier et al., 2020); however.

PA-12 aerosols generated for maternal inhalation exposure measured well within the size ranges of MNPs particles. The greatest number of particles within the aerosol samples were submicron (85.1 and 30.7 nm) in both particle electrical mobility (SMPS; Fig. 1a) and aerodynamic diameter (ELPI; Fig. 1b), respectively. Furthermore, the aerodynamic diameter (Fig. 1b) of these aerosols demonstrates a bimodal size distribution, shown by two distinct curves, with peaks at 30.7 nm and 3.81 μm.

PA-12 particles were identified in the tissues of male and female offspring at after gestational exposure, visualized in all of the offspring
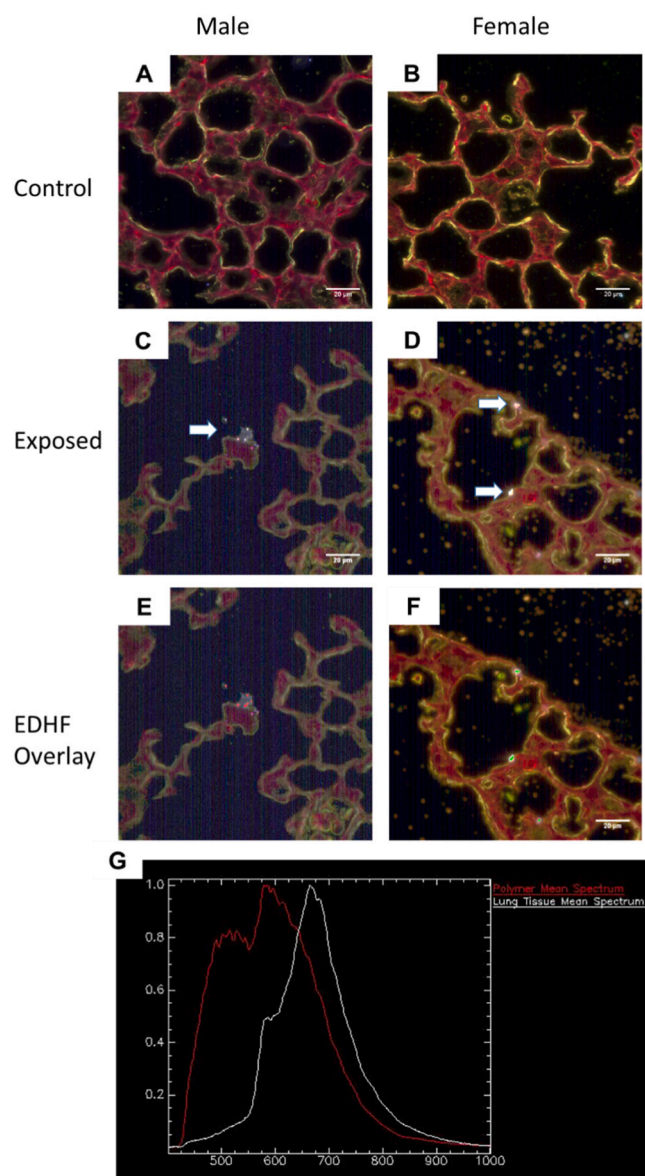

Fig. 2. Hyperspectral dark-field microscopy images of the offspring lung tissues for control male (A) and female (B) pups. Polyamide MNPs (white arrows) in the male (C) and female (D) offspring. Panels (E) and (F) apply the spectral EDHF SLF overlay to the male and female tissues, respectively. The wavelength spectra is presented in panel (G). No polyamide MNPs were identified in any (male or female) control pups. $n = 6$ (3 male/3 female) offspring representing 3 litters in each group.

Table 1
Litter characteristics of control and exposed dams.

	N	Maternal Weight (g)	Litter Size (n)	Neonatal Pup Weight (g)
Control	3	239 ± 6.66	10.33 ± 2.52	31.33 ± 2.75
Exposed	3	280 ± 26.06	8 ± 5.29	25.17 ± 7.29

tissues within the exposed group, including the lung (Fig. 2), heart (Fig. 3), liver (Fig. 4), kidney (Fig. 5), and brain (Fig. 6) of male (panels A, C, E) and female (panels B, D, F) pups harvested from exposed litters. There were no gross or microscopic histopathological changes noted between groups. There were no observable differences between male and female animals. There were no observable PA-12 particles within the tissues harvested from control pups. These images demonstrate the bio-persistence within a mammalian model.

4. Discussion and conclusion

This study exposed Sprague-Dawley rats to aerosolized PA-12, a representative MNP, during pregnancy. 2-weeks following delivery, PA-12 particles were visualized within the systemic tissues (e.g., lung, heart, liver, kidney, and brain) of representative male and female pups. While
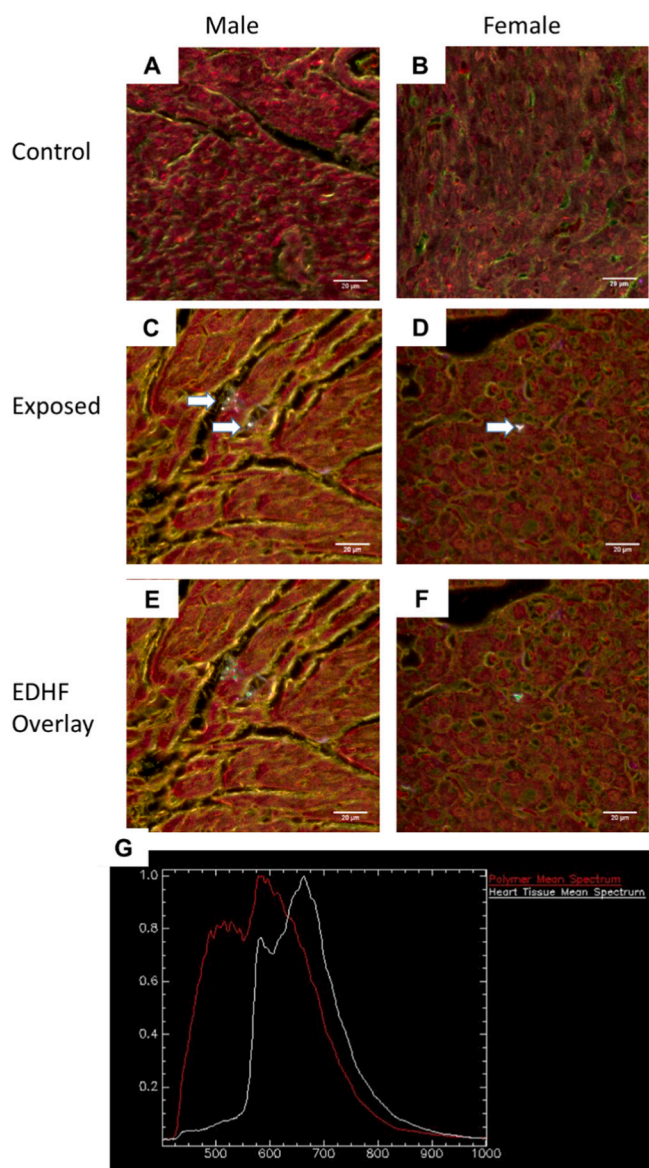

Fig. 3. Hyperspectral dark-field microscopy images of the offspring heart tissues for control male (A) and female (B) pups. Polyamide MNPs (white arrows) in the male (C) and female (D) offspring. Panels (E) and (F) apply the spectral EDHF SLF overlay to the male and female tissues, respectively. The wavelength spectra is presented in panel (G). No polyamide MNPs were identified in any (male or female) control pups. n = 6 (3 male/3 female) offspring representing 3 litters in each group.
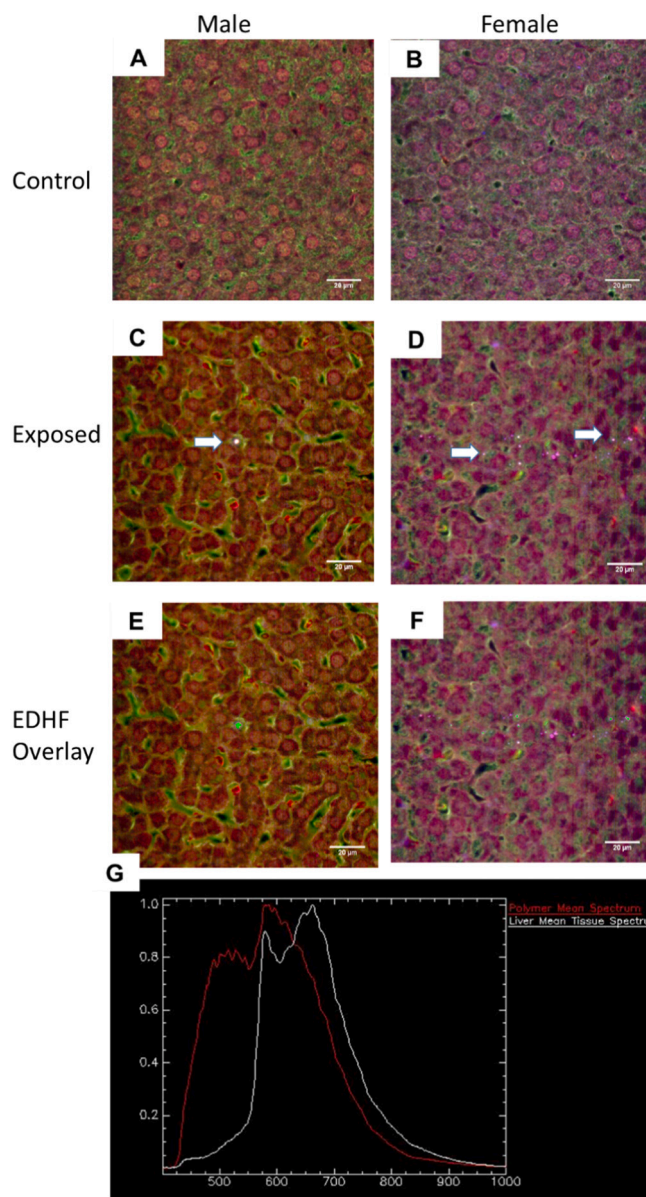

Fig. 4. Hyperspectral dark-field microscopy images of the offspring liver tissues for control male (A) and female (B) pups. Polyamide MNPs (white arrows) in the male (C) and female (D) offspring. Panels (E) and (F) apply the spectral EDHF SLF overlay to the male and female tissues, respectively. The wavelength spectra is presented in panel (G). No polyamide MNPs were identified in any (male or female) control pups. n = 6 (3 male/3 female) offspring representing 3 litters in each group.

previous studies have identified the maternal-fetal passage of MNP within 24 h of gastric or pulmonary exposure (Cary et al., 2023a; Fournier et al., 2020), this is the first study to demonstrate that these particles remain in offspring of the exposed dams, having deposited within the systemic tissues. Overall, these studies indicate that systemic bioaccumulation of MNP particles is maintained throughout neonatal development.

The Developmental Origins of Health and Disease (DOHaD) theory, previously coined *The Barker Hypothesis*, proposes that environmental exposures during gestation can predispose offspring to the development of disease later in life (Barker, 1990; Barker et al., 2010; Barker, 1999). Obesity, diabetes, cardiovascular, and metabolic diseases have been linked to early life exposure to environmental contaminants (Almeida et al., 2019; Haugen et al., 2015). Often these developmental outcomes
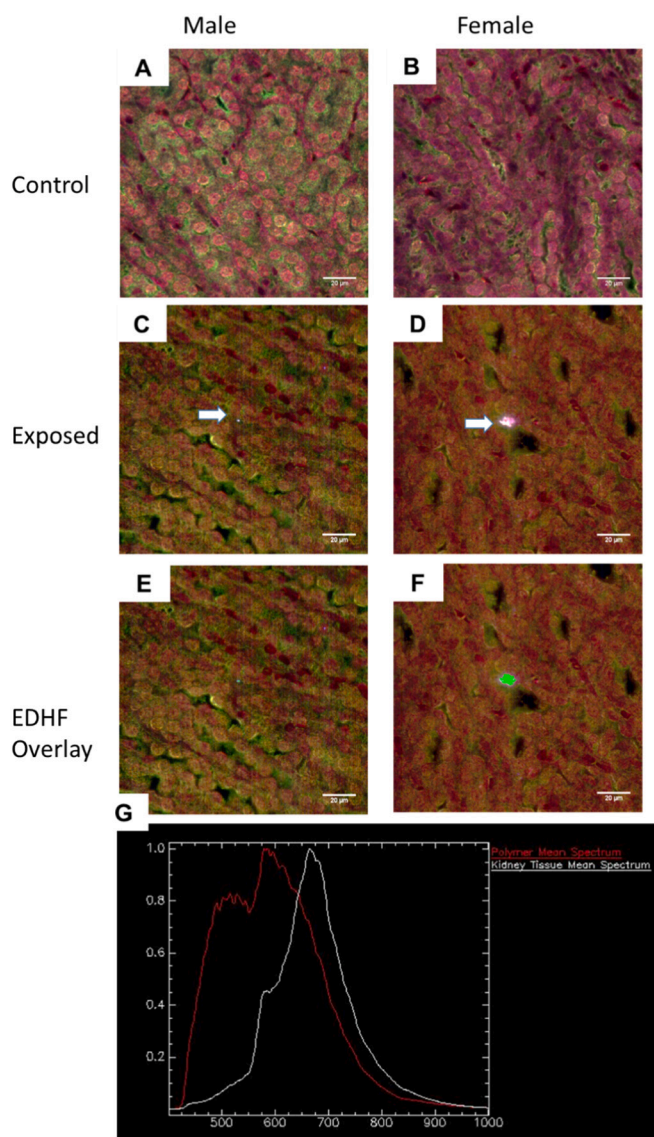
Fig. 5. Hyperspectral dark-field microscopy images of the offspring kidney tissues for control male (A) and female (B) pups. Polyamide MNPs (white arrows) in the male (C) and female (D) offspring. Panels (E) and (F) apply the spectral EDHF SLF overlay to the male and female tissues, respectively. The wavelength spectra is presented in panel (G). No polyamide MNPs were identified in any (male or female) control pups. n = 6 (3 male/3 female) offspring representing 3 litters in each group.

Fig. 6. Hyperspectral dark-field microscopy images of the offspring brain tissues for control male (A) and female (B) pups. Polyamide MNPs (white arrows) in the male (C) and female (D) offspring. Panels (E) and (F) apply the spectral EDHF SLF overlay to the male and female tissues, respectively. The wavelength spectra is presented in panel (G). No polyamide MNPs were identified in any (male or female) control pups. n = 6 (3 male/3 female) offspring representing 3 litters in each group.

are associated with fetal epigenetic modifications in response to environmental influences, including MNPs (Portha et al., 2014; Yu et al., 2021). As the deposition of MNP within systemic tissues has recently been associated with cardiovascular disease and inflammation (Marfella et al., 2024), it is probable the MNP deposition during early life may promote the development of disease.

In vitro exposure of human cells may provide mechanistic insight into potential MNP toxicity in developing fetuses and neonates. Human macrophages exposed to PA-12 had increased bioactivity at the endoplasmic reticulum-nucleus interface, cell-to-cell junctions, and within mitochondria (Alijagic et al., 2024). Furthermore, this exposure has been shown to stimulate genotoxicity, immunometabolism, and endocrine disruption in isolated human macrophages (Alijagic et al., 2024). Specifically, PA-12 led to a significant increase in IL-8 production, a key mediator produced by macrophages in the recruitment and activation of monocytes/neutrophils. 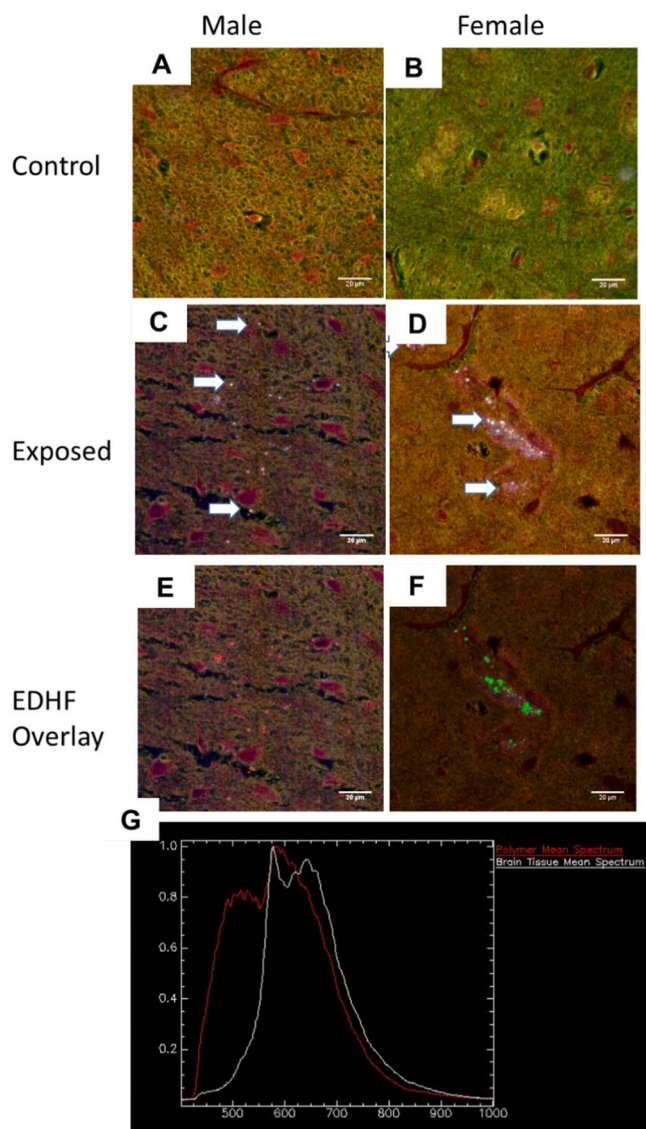Previous studies have also identified an association between local tissue inflammation and MNPs accumulation or deposition, which may have implications for the severity of cardiovascular or inflammatory bowel disease (Marfella et al., 2024; Yan et al., 2022). PA-12 exposure led to a significant reduction in bioavailable 17β-estradiol in estrus-stage female Sprague-Dawley rats after a single inhalation exposure, indicative of endocrine disruption (Cary et al., 2023b). In this study, we identified PA-12 micro-nanoparticles within the lung, heart, liver, kidney, and brain of male and female rat offspring, indirectly exposed via the pregnant and lactating mother. The long-term cellular effects and persistent health effects of MNPs deposition and bioaccumulation within developing offspring tissues remain to be elucidated.

Results of this study demonstrate maternal-to-fetal MNP translocation which remain in the independent 2-week old young pups. Unfortunately, we cannot discretely discern the MNPs introduced via gestational umbilical exposure from those passaged during lactation/nursing. Passage of the MNP via nursing and feeding would be

associated with maternally bioaccumulated particles during gestational exposure, which had ceased on GD 19. Therefore, studies utilizing a cross-foster design are warranted to determine the concentration of particles deposited within the offspring during gestational exposure from MNP passaged during lactation and feeding. As MNPs have also been identified in both human placenta (Garcia et al., 2024; Ragusa et al., 2021), fetal meconium (Braun et al., 2021; Liu et al., 2023a; Liu et al., 2023b; Zhang et al., 2021), and breastmilk (Ragusa et al., 2022), these findings highlight translational concerns of MNPs deposition and bioaccumulation within human infants.

The results presented within this study highlight the passage, biological accumulation, and permanence of MNP within the maternal-fetal model. These preliminary studies were not sufficiently powered to identify litter or sex differences between control/exposed groups or male/female pups; therefore, additional studies are underway to assess the development of fetal growth restriction after maternal MNP exposure, increased resorption sites, or sexually dimorphic outcomes. Furthermore, hyperspectral dark-field microscopy was utilized in these studies to solely identify the PA-12 particles within our tissue samples. We did not intend to quantify the representative MNP within these studies. The quantification of PA-12 within these tissues slices may be conducted in future studies and concentrations verified in combination with stimulated Raman spectroscopy (Qian et al., 2024) or pyrolysis-gas chromatography mass spectrometry (Garcia et al., 2024). Continued monitoring of MNP tissue deposition from neonate to adult, sourced only from maternal exposure during gestation and lactation, would provide substantiated data pertaining to the developmental onset of disease. Furthermore, an assessment of MNP particle mass balance, examining the tissue distribution from a known exposure concentration should be conducted. These studies need to be designed utilizing state-of-the-art analytical methodologies aimed specifically at the detection and quantification of nano-sized particles within biological matrices. In all, these results raise concerns for the toxicological impacts associated with MNPs exposure, maternal-fetal health, and systemic MNPs particle deposition.

CRediT authorship contribution statement

Gina M. Moreno: Writing – review & editing, Methodology, Investigation. **Tanisha Brunson-Malone:** Methodology, Investigation. **Samantha Adams:** Writing – review & editing, Methodology, Investigation. **Calla Nguyen:** Methodology, Investigation. **Talia N. Seymore:** Writing – review & editing, Methodology, Investigation. **Chelsea M. Cary:** Writing – review & editing, Methodology, Investigation. **Marianne Polunas:** Methodology, Investigation. **Michael J. Goedken:** Writing – review & editing, Methodology, Investigation. **Phoebe A. Stapleton:** Writing – original draft, Supervision, Resources, Methodology, Funding acquisition, Formal analysis, Data curation, Conceptualization.

Declaration of competing interest

The authors declare that they have no known competing financial interests or personal relationships that could have appeared to influence the work reported in this paper.

Data availability

Data will be made available on request.

References

Alijagic, A., Kotlyar, O., Larsson, M., Salihovic, S., Hedbrant, A., Eriksson, U., et al., 2024. Immunotoxic, genotoxic, and endocrine disrupting impacts of polyamide microplastic particles and chemicals. Environ. Int. 183, 108412.

Almeida, D.L., Pavanello, A., Saavedra, L.P., Pereira, T.S., de Castro-Prado, M.A.A., de Freitas Mathias, P.C., 2019. Environmental monitoring and the developmental origins of health and disease. J. Dev. Orig. Health Dis. 10, 608–615.

Amato-Lourenco, L.F., Carvalho-Oliveira, R., Junior, G.R., Dos Santos, Galvao L., Ando, R.A., Mauad, T., 2021. Presence of airborne microplastics in human lung tissue. J. Hazard. Mater. 416, 126124.

Antti-Poika, M., Nordman, H., Nickels, J., Keskinen, H., Viljanen, A., 1986. Lung disease after exposure to polyvinyl chloride dust. Thorax 41, 566–567.

Arkema, I., 2004. Technical Data Sheet, Orgasol ® NAT2. King of Prussia, Pennsylvania.

Arkema, I., 2021. Safety Data Sheet, Orgasol® 2001 NAT2. King of Prussia, Pennsylvania.

Baeza-Martinez, C., Olmos, S., Gonzalez-Pleiter, M., Lopez-Castellanos, J., Garcia-Pachon, E., Masia-Canuto, M., et al., 2022. First evidence of microplastics isolated in European citizens' lower airway. J. Hazard. Mater. 438, 129439.

Baldwin, A.K., Corsi, S.R., Mason, S.A., 2016. Plastic debris in 29 Great Lakes tributaries: relations to watershed attributes and hydrology. Environ. Sci. Technol. 50, 10377–10385.

Barker, D.J., 1990. The fetal and infant origins of adult disease. BMJ 301, 1111.

Barker, D.J., Thornburg, K.L. Osmond, C., Kajantie, E., Eriksson, J.G., 2010. Beyond birthweight: the maternal and placental origins of chronic disease. J. Dev. Orig. Health Dis. 1, 360–364.

Barker, D.J.P., 1999. Fetal origins of cardiovascular disease. Ann. Med. 31, 3–6.

Baron, P.A., Deye, G.J., Chen, B.T., Schwegler-Berry, D.E., Shvedova, A.A., Castranova, V., 2008. Aerosolization of single-walled carbon nanotubes for an inhalation study. Inhal. Toxicol. 20, 751–760.

Braun, T., Ehrlich, L., Henrich, W., Koeppel, S., Lomako, I., Schwabl, P., et al., 2021. Detection of microplastic in human placenta and meconium in a clinical setting. Pharmaceutics 13.

Cary, C.M., DeLoid, G.M., Yang, Z., Bitounis, D., Polunas, M., Goedken, M.J., et al., 2023a. Ingested polystyrene Nanospheres translocate to placenta and fetal tissues in pregnant rats: potential health implications. Nanomaterials (Basel) 13.

Cary, C.M., Seymore, T.N., Singh, D., Vayas, K.N., Goedken, M.J., Adams, S., et al., 2023b. Single inhalation exposure to polyamide micro and nanoplastic particles impairs vascular dilation without generating pulmonary inflammation in virgin female Sprague Dawley rats. Part. Fibre Toxicol. 20, 16.

Eschenbacher, W.L., Kreiss, K., Lougheed, M.D., Pransky, G.S., Day, B., Castellan, R.M., 1999. Nylon flock-associated interstitial lung disease. Am. J. Respir. Crit. Care Med. 159, 2003–2008.

Fournier, S.B., D'Errico, J.N., Adler, D.S., Kollontzi, S., Goedken, M.J., Fabris, L., et al., 2020. Nanopolystyrene translocation and fetal deposition after acute lung exposure during late-stage pregnancy. Part. Fibre Toxicol. 17, 55.

Fournier, S.B., Kallontzi, S., Fabris, L., Love, C., Stapleton, P.A., 2019. Effect of gestational age on maternofetal vascular function following single maternal engineered nanoparticle exposure. Cardiovasc. Toxicol. 19, 321–333.

Free, C.M., Jensen, O.P., Mason, S.A., Eriksen, M., Williamson, N.J., Boldgiv, B., 2014. High-levels of microplastic pollution in a large, remote, mountain lake. Mar. Pollut. Bull. 85, 156–163.

Garcia, M.A., Liu, R., Nihart, A., El Hayek, E., Castillo, E., Barrozo, E.R., et al., 2024. Quantitation and identification of microplastics accumulation in human placental specimens using pyrolysis gas chromatography mass spectrometry. Toxicol. Sci. 199, 81–88.

Haugen, A.C., Schug, T.T., Collman, G., Heindel, J.J., 2015. Evolution of DOHaD: the impact of environmental health sciences. J. Dev. Orig. Health Dis. 6, 55–64.

Horvatits, T., Tamminga, M., Liu, B., Sebode, M., Carambia, A., Fischer, L., et al., 2022. Microplastics detected in cirrhotic liver tissue. EBioMedicine 82, 104147.

Jenner, L.C., Rotchell, J.M., Bennett, R.T., Cowen, M., Tentzeris, V., Sadofsky, L.R., 2022. Detection of microplastics in human lung tissue using muFTIR spectroscopy. Sci. Total Environ. 831, 154907.

Jin, M., Wang, X., Ren, T., Wang, J., Shan, J., 2021. Microplastics contamination in food and beverages: direct exposure to humans. J. Food Sci. 86, 2816–2837.

Junaid, M., Hamid, N., Liu, S., Abbas, Z., Imran, M., Haider, M.R., et al., 2024. Interactive impacts of photoaged micro(nano)plastics and co-occurring chemicals in the environment. Sci. Total Environ. 927, 172213.

Kosuth, M., Mason, S.A., Wattenberg, E.V., 2018. Anthropogenic contamination of tap water, beer, and sea salt. PLoS One 13, e0194970.

Lenaker, P.L., Baldwin, A.K., Corsi, S.R., Mason, S.A., Reneau, P.C., Scott, J.W., 2019. Vertical distribution of microplastics in the water column and surficial sediment from the Milwaukee River basin to Lake Michigan. Environ. Sci. Technol. 53, 12227–12237.

Leslie, H.A., van Velzen, M.J.M., Brandsma, S.H., Vethaak, A.D., Garcia-Vallejo, J.J., Lamoree, M.H., 2022. Discovery and quantification of plastic particle pollution in human blood. Environ. Int. 163, 107199.

Liao, Z., Ji, X., Ma, Y., Lv, B., Huang, W., Zhu, X., et al., 2021. Airborne microplastics in indoor and outdoor environments of a coastal city in eastern China. J. Hazard. Mater. 417, 126007.

Liu, S., Guo, J., Liu, X., Yang, R., Wang, H., Sun, Y., et al., 2023a. Detection of various microplastics in placentas, meconium, infant feces, breastmilk and infant formula: a pilot prospective study. Sci. Total Environ. 854, 158699.

Liu, S., Liu, X., Guo, J., Yang, R., Wang, H., Sun, Y., et al., 2023b. The association between microplastics and microbiota in placentas and meconium: the first evidence in humans. Environ. Sci. Technol. 57, 17774–17785.

Marfella, R., Prattichizzo, F., Sardu, C., Fulgenzi, G., Graciotti, L., Spadoni, T., et al., 2024. Microplastics and Nanoplastics in Atheromas and cardiovascular events. N. Engl. J. Med. 390, 900–910.

Massardo, S., Verzola, D., Alberti, S., Caboni, C., Santostefano, M., Eugenio Verrina, E., et al., 2024. MicroRaman spectroscopy detects the presence of microplastics in human urine and kidney tissue. Environ. Int. 184, 108444.

Mitrano, D.M., Wick, P., Nowack, B., 2021. Placing nanoplastics in the context of global plastic pollution. Nat. Nanotechnol. 16, 491–500.

Portha, B., Fournier, A., Kioon, M.D., Mezger, V., Movassat, J., 2014. Early environmental factors, alteration of epigenetic marks and metabolic disease susceptibility. Biochimie 97, 1–15.

Qian, N., Gao, X., Lang, X., Deng, H., Bratu, T.M., Chen, Q., et al., 2024. Rapid single-particle chemical imaging of nanoplastics by SRS microscopy. Proc. Natl. Acad. Sci. 121, e2300582121.

Ragusa, A., Notarstefano, V., Svelato, A., Belloni, A., Gioacchini, G., Blondeel, C., et al., 2022. Raman microspectroscopy detection and characterisation of microplastics in human breastmilk. Polymers (Basel) 14.

Ragusa, A., Svelato, A., Santacroce, C., Catalano, P., Notarstefano, V., Carnevali, O., et al., 2021. Plasticenta: first evidence of microplastics in human placenta. Environ. Int. 146, 106274.

Schwabl, P., Köppel, S., Königshofer, P., Bucsics, T., Trauner, M., Reiberger, T., et al., 2019. Detection of various microplastics in human stool: a prospective case series. Ann. Intern. Med. 171, 453–457.

Shojaei, S., Ali, M.S., Suresh, M., Upreti, T., Mogourian, V., Helewa, M., et al., 2021. Dynamic placenta-on-a-chip model for fetal risk assessment of nanoparticles intended to treat pregnancy-associated diseases. Biochim. Biophys. Acta Mol. basis Dis. 1867, 166131.

Stapleton, P.A., 2019. Toxicological considerations of nano-sized plastics. AIMS Environ Sci 6, 367–378.

Toussaint, B., Raffael, B., Angers-Loustau, A., Gilliland, D., Kestens, V., Petrillo, M., et al., 2019. Review of micro- and nanoplastic contamination in the food chain. Food Addit. Contam. Part A Chem. Anal. Control Expo. Risk Assess. 36, 639–673.

Yan, Z., Liu, Y., Zhang, T., Zhang, F., Ren, H., Zhang, Y., 2022. Analysis of microplastics in human feces reveals a correlation between fecal microplastics and inflammatory bowel disease status. Environ. Sci. Technol. 56, 414–421.

Yang, Y., Xie, E., Du, Z., Peng, Z., Han, Z., Li, L., et al., 2023. Detection of various microplastics in patients undergoing cardiac surgery. Environ. Sci. Technol. 57, 10911–10918.

Yu, C.W., Luk, T.C., Liao, V.H., 2021. Long-term nanoplastics exposure results in multi and trans-generational reproduction decline associated with germline toxicity and epigenetic regulation in Caenorhabditis elegans. J. Hazard. Mater. 412, 125173.

Zhang, J., Wang, L., Trasande, L., Kannan, K., 2021. Occurrence of polyethylene terephthalate and polycarbonate microplastics in infant and adult feces. Environ. Sci. Technol. Lett. 8, 989–994.